Monthly Notices
of the
ROYAL ASTRONOMICAL SOCIETY

MNRAS **460,** 3587–3597 (2016)
Advance Access publication 2016 May 20

doi:10.1093/mnras/stw1212

The evolution of the equivalent width of the Hα emission line and specific star formation rate in star-forming galaxies at $1 < z < 5$

E. Mármol-Queraltó,[1⋆] R. J. McLure,[1⋆] F. Cullen,[1] J. S. Dunlop,[1] A. Fontana[2] and D. J. McLeod[1]

[1]*SUPA†, Institute for Astronomy, University of Edinburgh, Royal Observatory, Edinburgh EH9 3HJ, UK*
[2]*INAF–Osservatorio Astronomico di Roma, Via Frascati 33, Monte Porzio Catone, I-00040 Rome, Italy*

Accepted 2016 May 18. Received 2016 March 12; in original form 2015 November 6

ABSTRACT

We present the results of a study which uses spectral energy distribution (SED) fitting to investigate the evolution of the equivalent width (EW) of the Hα emission line in star-forming galaxies over the redshift interval $1 < z < 5$. After first demonstrating the ability of our SED-fitting technique to recover EW(Hα) using a sample of galaxies at $z \simeq 1.3$ with EW(Hα) measurements from 3D-HST grism spectroscopy, we proceed to apply our technique to samples of spectroscopically confirmed and photometric-redshift selected star-forming galaxies at $z \geq 1$ in the CANDELS (Cosmic Assembly Near-IR Deep Extragalactic Legacy Survey) UDS and GOODS-S fields. Confining our analysis to a constant stellar mass range ($9.5 < \log(M_{\star}/\mathrm{M}_{\odot}) < 10.5$), we find that the median EW(Hα) evolves only modestly with redshift, reaching a rest-frame value of EW(Hα) $=301 \pm 30$ Å by redshift $z \simeq 4.5$. Furthermore, using estimates of star formation rate (SFR) based on both UV luminosity and Hα line flux, we use our galaxy samples to compare the evolution of EW(Hα) and specific star formation rate (sSFR). Our results indicate that over the redshift range $1 < z < 5$, the evolution displayed by EW(Hα) and sSFR is consistent, and can be adequately parametrized as $\propto (1+z)^{1.0 \pm 0.2}$. As a consequence, over this redshift range, we find that the sSFR and rest-frame EW(Hα) of star-forming galaxies with stellar masses $M_{\star} \simeq 10^{10}\,\mathrm{M}_{\odot}$ are related by EW(Hα)/Å $= (63 \pm 7) \times$ sSFR/Gyr^{-1}. Given the current uncertainties in measuring the SFRs of high-redshift galaxies, we conclude that EW(Hα) provides a useful independent tracer of sSFR for star-forming galaxies out to redshifts of $z = 5$.

Key words: galaxies: evolution – galaxies: high-redshift.

1 INTRODUCTION

Obtaining a full understanding of the physical processes underlying the cosmic evolution of star formation and stellar mass assembly remains a fundamental goal of extragalactic astronomy. Following the discovery of the so-called *main sequence* of star formation (Daddi et al. 2007; Elbaz et al. 2007; Noeske et al. 2007), large amounts of observational effort have been invested in exploring the form and evolution of the star formation rate (SFR)–$M_{\star}$ relation (e.g. Karim et al. 2011; Whitaker et al. 2012, 2014; Speagle et al. 2014). Although notable disagreements concerning the normalization and slope of the main sequence still persist in the literature, it now seems likely that these are dominated by selection biases and that, if dealt with properly, the main sequence of star-forming galaxies has the form SFR $\propto M_{\star}^{0.7-1.0}$ out to redshifts of at least $z \simeq 3$ (e.g. Johnston et al. 2015; Renzini & Peng 2015), with a normalization which mirrors the cosmic evolution of SFR density (e.g. Madau & Dickinson 2014).

At high redshifts ($z \geq 2$), much of the attention in the recent literature has been focused on measuring the evolution of the specific star formation rate (sSFR), defined as the ratio of SFR to stellar mass (e.g. de Barros, Schaerer & Stark 2014; González et al. 2014; Koprowski et al. 2016; Tasca et al. 2015). Although there is clear consensus that the sSFR of typical star-forming galaxies rises rapidly from low redshift, reaching a value of $\simeq$2.5 Gyr^{-1} by $z \simeq 2$ (see Speagle et al. 2014 for a recent review), the evolution of sSFR at higher redshifts has been much more controversial. Initial studies (e.g. Stark et al. 2009; González et al. 2010) indicated that for galaxies with stellar masses of $\simeq 10^{10}\,\mathrm{M}_{\odot}$, sSFR remains approximately constant at $\simeq 2.5$ Gyr^{-1} over the redshift interval $2 < z < 6$. This result generated considerable interest, primarily because the apparent sSFR plateau is difficult to reconcile with

⋆ E-mail: emq@roe.ac.uk (EM-Q); rjm@roe.ac.uk (RJM)
† Scottish Universities Physics Alliance

theoretical expectations that sSFR should evolve $\propto (1+z)^{2.25}$, as it tracks the evolution of the gas accretion rate on to dark matter haloes (e.g. Neistein & Dekel 2008; Davé, Oppenheimer & Finlator 2011).

Given the potentially large systematic uncertainties that can affect stellar masses, and particularly SFRs, derived via spectral energy distribution (SED) fitting, it is obviously important to carefully consider the robustness of sSFR measurements at high redshift. Indeed, one systematic uncertainty which was not initially considered was the potential impact of nebular line emission. At high redshifts ($z \geq 4$), measurements of key stellar population parameters (i.e. age, stellar mass and SFR) are highly dependent on the strength of any photometric break between the available near-IR and mid-IR photometry. Unfortunately, there is a basic degeneracy in how best to model these photometric breaks with stellar population models. In most cases, it is possible to obtain acceptable fits using mature (e.g. $\simeq$300 Myr) stellar populations with moderate levels of star formation, where a Balmer break is fitted between the near-IR and mid-IR photometry. However, as indicated by Schaerer & de Barros (2009), it is often possible to obtain statistically identical (or improved) fits by invoking much younger ($\leq$50 Myr), lower mass stellar populations, with high SFRs and strong nebular line emission. In these SED fits, breaks between the near-IR and mid-IR photometry are typically the result of contamination of the mid-IR filters from strong [O III] or Hα line emission. In some cases, this basic degeneracy can lead to uncertainties in the estimated sSFR which are greater than an order of magnitude (e.g. Curtis-Lake et al. 2013).

In a recent study, de Barros et al. (2014) performed SED fitting on a sample of $\simeq$1700 Lyman-break galaxies (LBGs) at redshifts $3 < z < 6$, using stellar population models which included nebular emission. They concluded that $\simeq$65 per cent of LBGs display signs of significant nebular line emission and that SED fits incorporating nebular emission result in systematically lower stellar mass estimates and systematically higher SFR estimates. Although highly uncertain, de Barros et al. (2014) conclude that the sSFR evolves by a factor of 5–50 within the redshift interval $2 < z < 6$, more consistent with the theoretical expectations (factor of $\simeq$10 increase) than the results of González et al. (2010). However, when González et al. (2014) revisited the issue of how sSFR evolves at $z \geq 2$, they arrived at a markedly different conclusion. Even after incorporating nebular emission, González et al. (2014) find that the sSFR of galaxies with masses of $\sim 5 \times 10^9\,\mathrm{M}_\odot$ only increases by a factor of $\simeq$2.3 between $z = 2$ and 6, still in clear conflict with theoretical expectations.

The key to resolving this issue is obtaining a reliable measurement of the strength of nebular line emission in high-redshift galaxies. Within this context, the evolution of EW(Hα) is of particular interest because, in principle, it should provide an independent method for determining the sSFR. This follows from the fact that EW(Hα) is the ratio of a star formation indicator (Hα line flux) and a reasonable proxy for stellar mass (stellar continuum at $\lambda_{\rm rest} \simeq 6563$ Å). As a consequence, it is credible to expect some level of consistency between the redshift evolution of EW(Hα) and sSFR, although variation in the M/L ratios of star-forming galaxies at the youngest ages and highest SFRs could have an influence.

In fact, based on a combination of near-IR spectroscopy and narrow-band imaging, the recent literature presents a reasonably consistent picture of how EW(Hα) evolves out to $z \simeq 2$ (e.g. Erb et al. 2006; Fumagalli et al. 2012; Kashino et al. 2013; Sobral et al. 2013). However, the situation at higher redshifts is much less clear. Due to the lack of available mid-IR spectroscopy, at $z \geq 2.5$ it is currently only possible to measure EW(Hα) via the excess emission detected in the *Spitzer* IRAC 3.6 and 4.5 μm filters. In particular, the redshift interval $3.8 < z < 5.0$ represents a sweet-spot, where Hα contaminates the 3.6 μm filter but the 4.5 μm filter remains line free and suitable for anchoring SED-based continuum estimates.

Two previous studies have adopted an SED-based approach to measuring EW(Hα) at $3.8 < z < 5.0$. First, Shim et al. (2011) derived EW(Hα) measurements based on SED fits to the optical–mid-IR photometry for a final sample of 64 spectroscopically confirmed star-forming galaxies at $3.8 < z < 5.0$, *excluding* the contaminated 3.6 μm photometry from their SED fits. The results of the Shim et al. (2011) study suggested that galaxies with stellar masses of $\simeq 4 \times 10^9\,\mathrm{M}_\odot$ [converted to Chabrier initial mass function (IMF)] have a median EW(Hα) $\geq$ 600 Å, a factor of $\simeq$ 3 larger than EW(Hα) measurements at $z \simeq 2$ derived from near-IR spectroscopy (e.g. Erb et al. 2006). More recently, Stark et al. (2013) revisited this issue, using a final sample of 45 spectroscopically confirmed galaxies in the redshift interval $3.8 < z < 5.0$ (30 in common with Shim et al. 2011). Depending on whether they included or excluded the contaminated 3.6 μm photometry in their SED fitting, Stark et al. (2013) found that the typical value of EW(Hα) in their sample was in the range 270–410 Å.

Motivated by the continuing uncertainty over the evolution of EW(Hα), and how it relates to the evolution of the sSFR, in this paper we use SED fitting to consistently explore the evolution of EW(Hα) and sSFR over the redshift interval $1 < z < 5$. To achieve this, we analyse samples of spectroscopically confirmed star-forming galaxies at $1.20 < z < 1.50$, $2.10 < z < 2.45$ and $3.8 < z < 5.0$ in the CANDELS (Cosmic Assembly Near-IR Deep Extragalactic Legacy Survey) regions of the UDS and GOODS-S fields. In addition, we re-enforce our measurements of EW(Hα) at $z \geq 4$ by analysing a much larger sample of photometric-redshift selected star-forming galaxies at $3.8 < z_{\rm phot} < 5.0$. Within these three redshift windows, the Hα emission line contaminates the *Hubble Space Telescope* (*HST*) *F*160*W* (hereafter H_{160}), K_s and 3.6 μm filters, respectively. Consequently, it is clear that to accurately measure EW(Hα) at $z \geq 1$ based on SED fitting requires deep *K*-band data in combination with deep *and* accurately deconfused 3.6 μm+4.5 μm photometry.

Within this context, our study makes use of important new data sets that were previously unavailable. First, we exploit the photometry from the aperture-matched catalogues of the CANDELS UDS and GOODS-S fields (Galametz et al. 2013; Guo et al. 2013), which feature accurately deconfused IRAC fluxes extracted using the available H_{160}-band imaging as a high-resolution prior. Secondly, the UDS and GOODS-S CANDELS fields have recently been imaged to 5σ depths of 25.5–26.2(AB) in the K_s band by the HUGS survey (Fontana et al. 2014). Thirdly, we use our own reductions of the 3D-HST (Brammer et al. 2012) grism survey data covering the UDS and GOODS-S fields. In addition to providing spectroscopically confirmed star-forming galaxies within the traditional redshift desert ($1.5 < z < 2.5$), the 3D-HST data provide a sample of star-forming galaxies at $1.2 < z < 1.5$ with direct spectroscopic measurements of EW(Hα) with which to validate our SED-fitting technique.

The structure of the paper is as follows. In Section 2, we describe the photometric and spectroscopic data sets used in our analysis and our criteria for selecting a uniform sample of star-forming galaxies. In Section 3, we describe our SED-fitting technique for determining EW(Hα) and our adopted prescriptions for calculating stellar masses and SFRs. In Section 4, we describe the validation and calibration of our SED-fitting technique based on the 3D-HST

grism spectroscopy. In Section 5, we present our new EW(Hα) and sSFR results and compare them to recent studies in the literature. In Section 6, we explore the combined evolution of EW(Hα) and sSFR and discuss whether or not EW(Hα) can be used as a useful proxy for sSFR at high redshift. In Section 7, we present a summary of our main results and conclusions. Throughout the paper, we use the AB magnitude system (Oke 1974; Oke & Gunn 1983) and adopt the following cosmology: $\Omega_{\rm m} = 0.3$, $\Omega_{\Lambda} = 0.7$ and $H_0 = 70\,{\rm km\,s^{-1}\,Mpc^{-1}}$. Unless otherwise stated, we use EW(Hα) to refer to the rest-frame equivalent width throughout.

2 DATA

The analysis in this paper is based primarily on the photometry and spectroscopy of the UDS and GOODS-S fields provided by the public CANDELS (Grogin et al. 2011; Koekemoer et al. 2011) and 3D-HST spectroscopic surveys (Brammer et al. 2012), respectively. In common with all five of the CANDELS survey fields, the UDS and GOODS-S feature the deep optical, near-IR and *Spitzer* IRAC imaging necessary to trace the evolution of the EW(Hα) via SED fitting. However, crucially, amongst the CANDELS fields, it is *only* the UDS and GOODS-S which feature suitably deep K_s-band imaging, provided by the recently completed HUGS survey (Fontana et al. 2014).

2.1 CANDELS photometry

The success of this study relies on the quality of the available photometry, and for our purposes we have adopted the publicly available photometry catalogues of the CANDELS UDS and GOODS-S fields published by Galametz et al. (2013) and Guo et al. (2013). For the GOODS-S field, we make use of the update to the Guo et al. (2013) catalogue released by Fontana et al. (2014) which includes the final K_s-band photometry from the HUGS survey. Both catalogues are selected using the CANDELS H_{160} imaging and feature point spread function-matched isophotal photometry measured from the *HST* ACS and WFC3/IR imaging available across both fields. Likewise, both catalogues make use of the TFIT (Laidler et al. 2007) deconfusion package which utilizes H_{160} priors to obtain aperture-matched photometry in the available optical+near-IR ground-based imaging and *Spitzer* IRAC data. As highlighted above, the latest versions of both catalogues feature TFIT-generated photometry in the K_s band from the recently completed HUGS survey. Full details of how the photometry catalogues were generated can be found in Galametz et al. (2013) and Guo et al. (2013), respectively.

2.2 3D-HST spectroscopy

The 3D-HST survey provides low spectral resolution, spatially resolved, near-IR grism spectroscopy of all five of the CANDELS survey fields (Brammer et al. 2012). Specifically, the 3D-HST survey employs the G141 grism on WFC3/IR to provide spectra with $R \sim 130$ over the wavelength range 1.10–1.68 μm. The raw data from 3D-HST are publicly available, and we have employed our own modified version of the AXE software package (Kümmel et al. 2009) to reduce the data available over the UDS and GOODS-S fields. The grism spectra we employ here were originally reduced for the gas-phase metallicity study of Cullen et al. (2014), to which the reader is referred for further details of the reduction and redshift determination processes.

The 3D-HST spectra play a crucial role in validating our SED-fitting technique for measuring EW(Hα). In the redshift interval $1.2 < z < 1.5$, where the Hα emission line contaminates the H_{160} filter, the 3D-HST spectra cover both the [O III] and Hα emission lines. Consequently, within this redshift range, the 3D-HST spectra can provide both unambiguous spectroscopic redshifts and *direct* spectroscopic measurements of EW(Hα). In addition, the 3D-HST spectra are an excellent resource for obtaining emission-line redshifts of star-forming galaxies in the traditional redshift desert and provide many of the spectroscopically confirmed objects in our $z \simeq 2.3$ sub-sample where Hα contaminates the K_s filter.

2.3 Spectroscopic galaxy sample

In order to study the evolution of EW(Hα) at $z > 1$, we have assembled samples of spectroscopically confirmed star-forming galaxies in the redshift ranges: $1.2 < z < 1.5$, $2.1 < z < 2.45$ and $3.8 < z < 5.0$, where the Hα emission line contaminates the H_{160}, K_s and IRAC 3.6 μm filters, respectively. In addition to galaxies drawn from the 3D-HST survey, the initial samples were drawn from the various different spectroscopic studies of the GOODS-S and UDS fields: Cimatti et al. (2002), Le Fèvre et al. (2004), Mignoli et al. (2005), Vanzella et al. (2008), Popesso et al. (2009), Cooper et al. (2012), McLure et al. (2013) and Morris et al. (2015). Objects were only considered for selection if they had the highest quality spectroscopic redshift flags.

After the initial selection process, the final samples were restricted to those star-forming galaxies for which statistically acceptable SED fits were obtained at their spectroscopic redshifts, with corresponding stellar mass measurements lying in the range $9.5 < \log(M_{\star}/{\rm M}_{\odot}) < 10.5$ (see Section 3). Moreover, in order to exclude passive/quiescent systems, galaxies with UV-luminosity-based SFR estimates inconsistent with lying on the main sequence were also excluded. Although our final spectroscopic galaxy samples are clearly not complete, their location on the main sequence (see Section 5.1) demonstrates that they are fully representative of the dominant star-forming galaxy population at $1 < z < 5$ in the mass range $9.5 < \log(M_{\star}/{\rm M}_{\odot}) < 10.5$. The basic properties of the three spectroscopic star-forming galaxy samples are provided in Table 1.

2.4 Photometric galaxy sample

The two lower redshift galaxy samples at $z \simeq 1.3$ and $z \simeq 2.3$ are selected within sufficiently narrow redshift intervals (i.e. $\Delta z = 0.3$ and 0.35, respectively) that the necessity for spectroscopic redshifts is clear. However, the width of the IRAC 3.6 μm filter allows us to study the impact of Hα emission over the redshift range $3.8 < z < 5.0$ (i.e. $\Delta z = 1.2$). Moreover, the presence of a strong Lyman break in their spectra makes the selection of star-forming galaxies at these redshifts reasonably straightforward.

Consequently, in order to boost the statistics in our highest redshift bin, we assembled a sample of LBGs based on our own photometric-redshift analysis of the Fontana et al. (2014) and Galametz et al. (2013) catalogues. Applying the same stellar mass and sSFR criteria (and excluding the objects in common with the $z \simeq 4$–5 spectroscopic sample), the final sample of photometric-redshift selected galaxies comprises 129 objects in the redshift range $3.8 < z_{\rm photo} < 5.0$. The basic properties of the final photometric sample of star-forming galaxies are also shown in Table 1. The good agreement between the median properties inferred for the photometric and spectroscopic samples of galaxies at $3.8 < z < 4.5$ is notable, confirming that the spectroscopic sample is not a biased sub-set of star-forming galaxies in this redshift range. For that

Table 1. Summary of the measured and derived properties of the four different galaxy samples analysed in this study. Column 1 lists the sample name and column 2 lists the number of objects within each sample. The final sample in the table is simply the combination of the spectroscopic and photometric-redshift selected samples at $z \simeq 4.5$. Columns 3 and 4 list the median redshift and median stellar mass for each sample. Column 5 lists the median rest-frame EW of the Hα emission line as derived from our SED fitting. Columns 6 and 7 list the median values of sSFR, as derived from the rest-frame UV and the measured EW(Hα), respectively (see the text for full details).

Sample	N	z	$\log(M_\star/\mathrm{M}_\odot)$	EW(Hα)/Å	sSFR_UV/Gyr^{-1}	sSFR_Hα/Gyr^{-1}
spec-z ($1.2 < z < 1.5$)	143	1.34	9.83	146 ± 9	2.0 ± 0.2	1.7 ± 0.2
spec-z ($2.1 < z < 2.5$)	71	2.25	9.77	217 ± 17	4.0 ± 0.3	4.5 ± 0.3
spec-z ($3.8 < z < 5.0$)	26	4.55	9.79	288 ± 92	4.3 ± 0.6	5.5 ± 1.1
phot-z ($3.8 < z < 5.0$)	129	4.34	9.69	313 ± 29	5.4 ± 0.3	5.1 ± 0.6
full ($3.8 < z < 5.0$)	155	4.38	9.70	301 ± 30	5.3 ± 0.3	5.4 ± 0.5

reason, from now on we will quote the values for the full sample (i.e. phot-z + spec-z) when referring to this redshift range.

3 EWS, STELLAR MASSES AND SFRS

In this section, we describe our SED-fitting technique for measuring EW(Hα) from the available multiwavelength photometry. We also describe our adopted prescriptions for calculating the stellar masses and SFRs of the galaxies in our spectroscopic and photometric samples.

3.1 SED fitting

The photometry for all objects included in this study was analysed using the template-fitting software described in McLure et al. (2011). A fuller description of the latest version of this software is provided in McLeod et al. (2015), but we provide the essential details here for completeness. The standard version of the code uses Bruzual & Charlot (2003, hereafter BC03) SED templates, combined with the Calzetti et al. (2000) dust attenuation law and the Madau (1995) prescription for IGM absorption. Strong nebular emission lines can be included in the template fitting, with the Hα line flux calculated from the template SFR and the strength of other significant nebular lines set using the line ratios determined by Cullen et al. (2014). The template fitting is performed in flux space to allow the proper treatment of flux errors and, in addition to photometric redshifts, the code delivers best-fitting values of stellar mass, SFR and synthetic photometry for the best-fitting template.

Throughout the SED-fitting process, we adopted BC03 stellar evolutionary models with solar and sub-solar metallicities ($\mathrm{Z}_\odot$, $0.5\,\mathrm{Z}_\odot$ and $0.2\,\mathrm{Z}_\odot$), a Chabrier IMF and a range of star formation histories with exponentially decaying SFRs (τ-models) in the range $0.2 < \tau < 10$ Gyr. In obtaining the best-fitting SED, dust attenuation was allowed to vary over the range $0 < A_V < 2.5$ and template ages were required to be between 50 Myr and the age of the Universe at a given redshift.

3.2 EW and stellar mass

Two separate SED fits were performed for each object, in both cases fixing the redshift to the spectroscopic value (or best-fitting z_{phot} value for the photometrically selected $z \simeq 4.5$ sample) and adopting the same set of SED templates.

In the first SED fit, all of the available multiwavelength photometry was included and nebular emission lines were added to the SED templates. It is the best-fitting values of stellar mass returned by these SED fits which are adopted throughout the subsequent analysis. In contrast, during the second SED fit, all filters potentially contaminated by strong nebular emission lines (i.e. [O II], [O III] or Hα) were *excluded* from the fit. The results of this SED fit are used to calculate the rest-frame EW of the Hα emission line via the formula

$$\mathrm{EW} = \frac{W_{\mathrm{rec}}}{(1+z)}\left(10^{(-0.4\Delta\mathrm{mag})} - 1\right), \quad (1)$$

where W_{rec} is the rectangular width of the filter contaminated by Hα and Δmag is the difference between the observed magnitude in that filter and the synthetic magnitude from the SED fit excluding filters potentially contaminated by strong line emission (i.e. $\Delta\mathrm{mag} = m_{\mathrm{obs}} - m_{\mathrm{SED}}$). As previously discussed, in this study we consider Hα contamination of the H_{160}, K_s and IRAC 3.6 µm filters for galaxies at $z \simeq 1.3$, $z \simeq 2.3$ and $z \simeq 4.5$. For these three filters, we adopt W_{rec} values of 2683, 3150 and 6844 Å, respectively. In reality, the SED fits return a measurement of the total EW of all the emission lines within the relevant filter (i.e. Hα, [N II] and [S II]). In Section 4, we calibrate for this effect by comparing our SED-based results with direct spectroscopic EW measurements.

As an illustration of how the SED-fitting method works, Fig. 1 shows the stacked multiwavelength photometry and the stacked best-fitting SED templates for the spectroscopically confirmed galaxies at $z \simeq 2.3$ (left-hand panel) and $z \simeq 4.5$ (right-hand panel) in the GOODS-S field. Compared to the best-fitting SED templates (fitted by excluding filters potentially contaminated by line emission), the excess flux in the K_s and IRAC 3.6 µm filters, caused by Hα emission at $z \simeq 2.3$ and $z \simeq 4.5$ respectively, is clearly visible.

3.3 Star formation rate

When combined with spectroscopic redshifts, the high S/N ratio UV–mid-IR data available within the UDS and GOODS-S CANDELS fields provide SED-based stellar mass measurements which are relatively well constrained (e.g. Mobasher et al. 2015). Indeed, the median stellar masses of our four galaxy samples (see Table 1) are stable at the ± 0.15 dex level, irrespective of the allowed range in metallicity, reddening and star formation time-scale (or indeed, whether filters contaminated by line emission are included or excluded).

Unfortunately, however, the estimates of SFR derived from SED fitting are far less stable, showing large discrepancies depending on the adopted dust reddening, metallicity and star formation histories. As a result, adopting different modelling assumptions, it is perfectly possible to obtain statistically acceptable SED fits to our samples of $1 < z < 5$ star-forming galaxies which result in median sSFR values which differ by a factor of $\simeq$4. Consequently, throughout the analysis presented in this paper, we have adopted two different, semi-empirical, estimates of SFR, both of which have the benefit of being largely independent of the adopted set of SED templates.

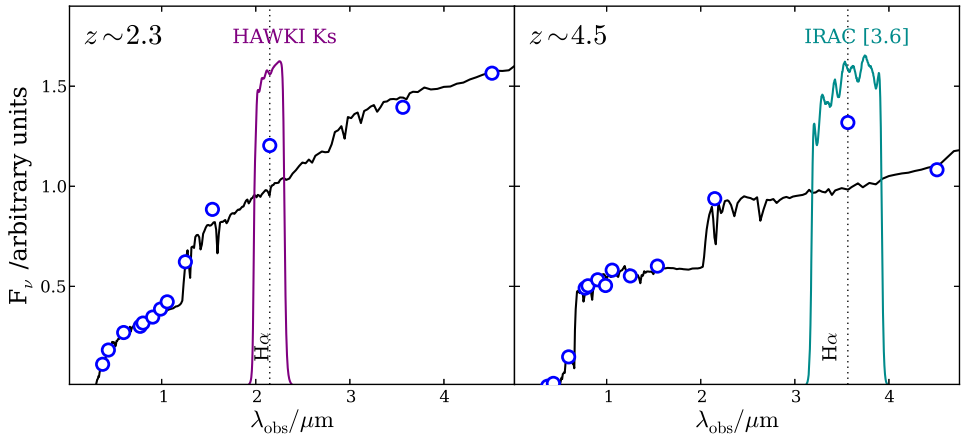

Figure 1. The left-hand panel shows the stacked multiwavelength photometry for the galaxies in the $2.1 < z < 2.45$ spectroscopic sample drawn from the GOODS-S field. The solid black line shows a stack of the best-fitting SED templates (derived by excluding filters contaminated by strong emission lines from the fitting process). The purple line indicates the transmission profile of the K_s-band filter, which should be contaminated by the Hα emission line at these redshifts. The stacked K_s-band photometry shows a clear excess in comparison to the stacked SED templates (it can also be seen that the H_{160} filter is contaminated by [O III] emission). The right-hand panel shows the equivalent information for the $z \simeq 4.5$ spectroscopic galaxy sample. In this case, a clear flux excess due to Hα emission can be seen in the IRAC 3.6 μm filter (turquoise line).

3.3.1 UV SFR estimate

Our primary SFR estimate is based on the far-UV luminosity of each galaxy, as measured from the best-fitting SED template (excluding line-contaminated filters) using a 100-Å-wide top-hat filter centred on $\lambda_{rest} = 1500$ Å. To calculate the reddening, we have derived the UV spectral slope (β) of each galaxy using top-hat filters centred on 1410 and 2400 Å, corresponding to UV windows no. 4 and 10 from Calzetti, Kinney & Storchi-Bergmann (1994). Based on the derived values of β, the dust reddening was then calculated using the Meurer, Heckman & Calzetti (1999) correlation between dust extinction (A_{1600}) and β. Once the 1500 Å luminosities were dust corrected [assuming $A_{1500} = 1.04A_{1600}$, as predicted by the Calzetti et al. (2000) attenuation law], the final SFR estimates were derived using the updated correlation between UV luminosity and SFR adopted by Madau & Dickinson (2014):

$$\log(\mathrm{SFR}) = \log(L_{1500}) - 28.14, \quad (2)$$

where SFR is measured in $M_\odot$ yr^{-1}, L_{1500} is measured in erg s^{-1} Hz^{-1} and we have corrected from a Salpeter to a Chabrier IMF assuming a correction factor of 0.63.

3.3.2 Hα SFR estimate

The second SFR estimate is based on the Hα line flux of each galaxy, as derived from the corresponding EW(Hα) measurement. In performing this calculation, the continuum flux is estimated from the best-fitting SED template (excluding line-contaminated filters) using a 100-Å-wide top-hat filter centred on $\lambda_{rest} = 6563$ Å. Moreover, the Hα fluxes are dereddened assuming $A_{6563} = 0.33A_{1600}$, as predicted by the Calzetti et al. (2000) reddening law where, as before, A_{1600} is derived using the A_{1600}–β correlation from Meurer et al. (1999). This calculation therefore explicitly assumes that the nebular and continuum reddening are identical, as found in a recent study of 3D-HST star-forming galaxies at $z \simeq 2.2$ by Cullen et al. (2014), and consistent with the recent work by Reddy et al. (2015) for galaxies with our median mass and SFR. We have adopted the following relationship between Hα luminosity and SFR:

$$\log(\mathrm{SFR}) = \log(L_{H\alpha}) - 41.35, \quad (3)$$

where SFR is measured in $M_\odot$ yr^{-1} and $L_{H\alpha}$ is measured in erg s^{-1}. We note that this calibration produces SFR estimates ∼10 per cent lower than the recent calibration of Kennicutt & Evans (2012) and ∼10 per cent higher than the calibration of Madau, Pozzetti & Dickinson (1998), when both are corrected to a Chabrier IMF.

4 TESTING THE SED-FITTING METHOD

Before proceeding to present the main results, in this section we provide details of the tests which were performed to validate and calibrate our SED-fitting technique for measuring EW(Hα). All of the tests were performed using a sample of star-forming galaxies at $z \simeq 1.3$, drawn from the 3D-HST sample in the UDS and GOODS-S fields. As previously discussed, these galaxies are ideal for our purposes because they allow a comparison of the SED-based EW measurements with direct measurements from the 3D-HST spectra.

4.1 Individual 3D-HST spectra

The Hα emission line lies securely within the H_{160} filter for galaxies within the redshift interval $1.2 < z < 1.5$. Consequently, our initial sample consisted of all galaxies within this redshift range, with high S/N ratio detections of the Hα emission line. In addition, we also required that the 3D-HST spectra provided unambiguous spectroscopic redshifts (effectively meaning that [O III] 5007 was also detected) and a continuum detection free from significant contamination due to overlapping spectra from nearby objects. After applying these criteria, the final test sample consisted of 48 galaxies with redshifts in the range $1.23 < z < 1.49$.

The individual spectra were fitted with a combination of a linear continuum and two Gaussians to reproduce the blended [O III] doublet, Hα and [N II] emission lines. After subtracting the continuum, the fluxes of the blended Hα+[N II] emission lines were measured within $\pm 3\sigma$ from the centroid of the best-fitting Gaussian, and EW(Hα) was calculated under the assumption that Hα contributes 90 per cent of the total Hα+[N II] flux (taken from Sanders et al. 2015, for star-forming galaxies with similar SFRs in our stellar mass range). To estimate the error in derived EW

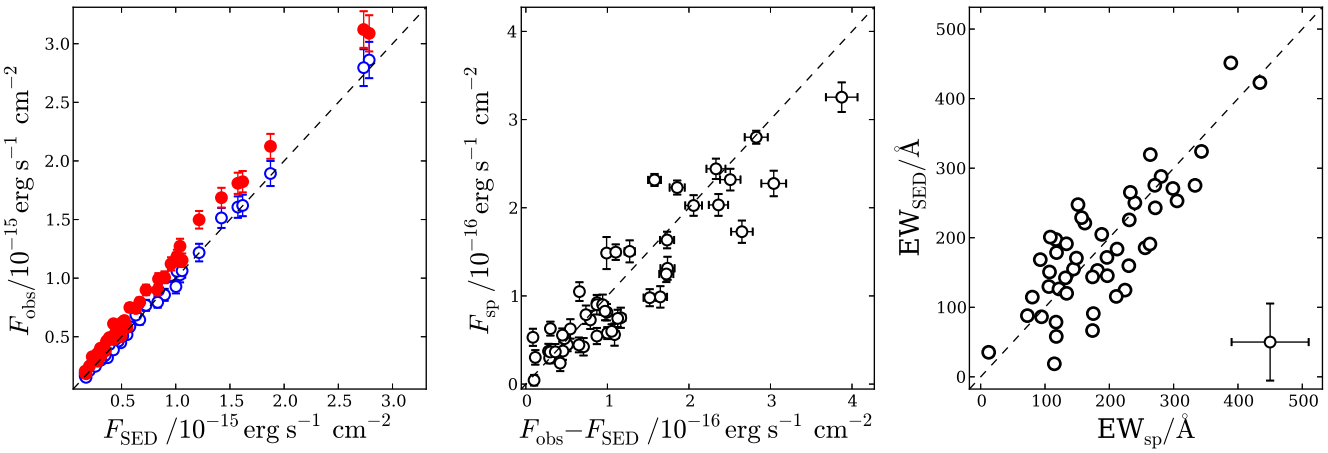

Figure 2. Each panel shows data for the final sample of 48 galaxies at $z \simeq 1.3$ for which it was possible to extract reliable measurements of EW(Hα) from their 3D-HST spectra. In each panel, the dashed line indicates a 1:1 relation. The left-hand panel compares the average continuum flux calculated from the observed H_{160} magnitude (filled red circles) with the continuum flux predicted by SED fitting of the multiwavelength photometry, excluding filters contaminated by strong emission lines. The open blue data points show the continuum flux measured from the observed H_{160} magnitude, after subtracting the Hα line flux measured from the 3D-HST spectra. The middle panel shows the Hα line flux as measured from the spectra versus the line flux predicted from the difference between the observed and synthetic H_{160} magnitudes. As expected, the predicted line flux is $\simeq$20 per cent larger than the measured Hα line flux, simply because the raw output from the SED fitting is a measurement of the flux of all emission lines within the H_{160} filter (i.e. Hα+[N II]+[S II]). The right-hand panel shows EW(Hα) derived from the SED fitting versus EW(Hα) measured from the 3D-HST spectra. Under the assumption that there should exist a 1:1 relation between the two, the EW$_{\rm SED}$ values have been scaled by a factor of $f = 0.9$ (see the text for details). A representative error bar, computed as the median value of the individual error bars for each galaxy, is shown in the lower-right corner.

measurements, a set of 100 realizations was run, in which the 3D-HST spectrum is perturbed according to its error spectrum.

The results of the SED-fitting tests on the final sample of 48 test galaxies at $z \simeq 1.3$ are shown in Fig. 2. In the left-hand panel, the average continuum flux calculated from the observed H_{160} magnitude (red data points) is plotted against the continuum flux calculated from the synthetic H_{160} magnitude returned by the best-fitting SED template (excluding filters potentially contaminated by line emission). As expected, a clear flux excess is apparent. In contrast, the blue data points show the average continuum flux after the observed H_{160} photometry has been corrected by subtracting the emission-line flux measured from the 3D-HST spectra. As can clearly be seen, the two continuum estimates are now in excellent agreement. The middle panel of Fig. 2 shows the Hα line flux measured from the 3D-HST spectra versus the Hα line flux estimated from the difference between the observed and synthetic H_{160} photometry. It can be seen that the two independent Hα line flux measurements are well correlated, with a tendency for the SED-based estimate to be systematically $\simeq$20 per cent higher. Again, this is as expected, given that the SED-based results inevitably yield an estimate of the total Hα+[N II]+[S II] line flux.

Finally, the right-hand panel of Fig. 2 shows EW(Hα) measured from the SED fitting, versus EW(Hα) measured from the 3D-HST spectra. To produce the final calibration of the relationship between the SED-based EW measurements and the direct spectroscopic measurements, we have explicitly assumed that there should exist a 1:1 relation between the two, and that the only freedom should be to introduce a multiplicative factor (f) in order to correct the SED-based measurements for the additional flux of the [N II] and [S II] emission lines. Under this assumption, it was found that scaling the SED-based EW measurements by $f = 0.9$ produced the best reproduction of the EW measurements from the 3D-HST spectra. As demonstrated by the right-hand panel of Fig. 2, based on this scaling, the SED-based and spectroscopically measured EWs follow a 1:1 relation. Unless otherwise stated, all EW(Hα) measurements based on SED fitting quoted in this paper have been scaled by $f = 0.9$ according to this calibration.

4.2 Stacked 3D-HST spectra

Having demonstrated the validity of our SED-based technique for measuring EW(Hα) on individual objects, an additional test was performed on the median stack of the 48 spectra from the test sample. For those 48 galaxies, we first normalized their spectrum to the region $\lambda = 5200$–6250 Å before calculating a median stack. The resulting stacked spectrum is shown in Fig. 3, along with the best-fitting emission-line plus continuum model.

The measured value of EW(Hα+[N II]) from the stacked spectra is 189 $\pm$ 19 Å. Assuming that Hα contributes 90 per cent of the Hα+[N II] flux (Sanders et al. 2015), the stacked spectrum therefore indicates a median EW(Hα) of 170 $\pm$ 17 Å. In the inset, the distribution of EW(Hα) measurements from the SED fits to the 48 individual galaxies is shown as a histogram. The median value of the individual EW(Hα) determinations is 175 $\pm$ 14 Å, in excellent agreement with the value measured from the stacked spectra.

Although in the individual spectra it is not possible to reliably fit Hβ and [S II] $\lambda\lambda$6717, 6731 for most of the galaxies, these emission lines are clear in the stacked spectra. As can be seen from the results reported in Fig. 3, we find that, on average, $\simeq$12 per cent of the [S II]+Hα+[N II] flux is contributed by [S II].

5 RESULTS

We now present our new results on both sSFR and EW(Hα) and compare them with recent results in the literature. The basic results are tabulated in Table 1 and plotted in Figs 4 and 5.

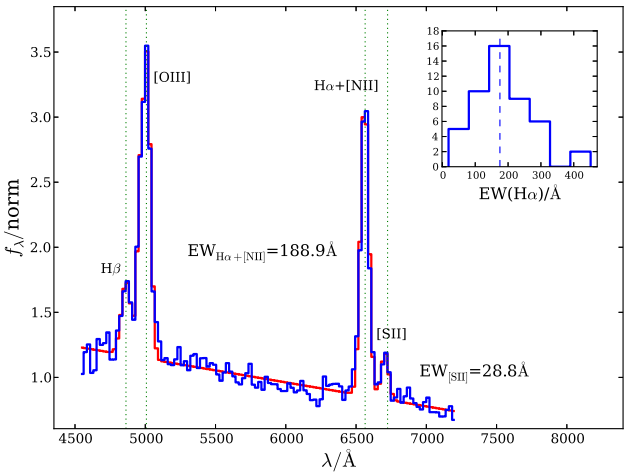

Figure 3. The median stack of the 3D-HST spectra for the 48 galaxies at $z \simeq 1.3$ featured in Fig. 2 is shown in blue. The red line shows the best-fitting continuum+emission-line model. The measured value of EW(Hα+[N II]) from the stacked spectrum is 189 ± 19 Å. Assuming that Hα contributes 90 per cent of the Hα+[N II] flux (Sanders et al. 2015), the stacked spectrum therefore indicates a median EW(Hα) of 170 ± 17 Å. The inset shows the distribution of EW(Hα) measurements from our SED fitting of the individual objects that went into the stack. The median value of the individual EW(Hα) measurements returned by the SED fitting is 175 ± 14 Å, in excellent agreement with the value measured from the stacked spectra.

5.1 The evolution of sSFR

Before discussing our new EW(Hα) results, it is of interest to explore our determinations of sSFR within the context of recent literature studies. This serves two purposes. First, it is an opportunity to confirm that our adopted methods for estimating sSFR are at least in reasonable agreement with previous studies, and that our four galaxy samples are representative of main-sequence galaxies within the redshift interval of interest. Secondly, if there is a close link between the evolution of sSFR and EW(Hα), the apparent evolution of sSFR with redshift should provide a template for the redshift evolution of EW(Hα).

In Fig. 4, we plot median sSFR against redshift for our four galaxy samples. In each case, we plot two values of sSFR, one where the SFR is based on the dust-corrected UV luminosities and one where SFR is based on the Hα line fluxes corresponding to the EW(Hα) measurements. In this figure, we have also plotted the results from a selection of sSFR studies in the literature for comparison. To provide a fair comparison, for those studies at $z \leq 4$, we have corrected the sSFR values to a common stellar mass of $\log_{10}(M_\star/\,\mathrm{M}_\odot) = 9.8$ (Chabrier IMF) based on the prescription of Dutton, van den Bosch & Dekel (2010). For those literature studies at $z \geq 4$, the median masses of the galaxy samples should be sufficiently close to $\log_{10}(M_\star/\,\mathrm{M}_\odot) = 9.8$ to make any correction unnecessary. The exception to this is the sSFR data point from Rasappu et al. (2015), which we have plotted as a down arrow simply because it is based on a galaxy sample with a significantly lower median stellar mass (see Section 5.3.3). Finally, in Fig. 4, we also plot three different curves. The first (green dashed line) is the sSFR–z relation for galaxies with stellar mass of $\log_{10}(M_\star/\,\mathrm{M}_\odot) = 9.8$ from the meta-analysis of 25 different literature main-sequence studies by Speagle et al. (2014). The second (black dotted line) is the theoretical expectation that $\mathrm{sSFR}(z) \propto (1+z)^{2.25}$, normalized to pass through the cluster of sSFR data points within the redshift range $1 < z < 2$. The final curve (blue solid line) is the best-fitting sSFR–z relationship of the form $\propto (1+z)^{1.0}$, as derived by fitting to our new data points alone, and is therefore valid at $z > 1$. This sSFR–z relationship is suggested by considering the evolution of EW(Hα) and sSFR together, and is discussed further in Section 6.

Two points are immediately clear from Fig. 4. First, it can be seen that our sSFR estimates based on EW(Hα) are very consistent with the corresponding sSFR estimates based on UV luminosity. Secondly, it can be seen that both sSFR determinations are perfectly consistent with the sSFR–z relation for galaxies with stellar mass of $\log_{10}(M_\star/\,\mathrm{M}_\odot) = 9.8$ from Speagle et al. (2014), which also provides a good description of the literature sSFR data over the full $0 < z < 7$ redshift range. We can therefore be confident that our galaxy samples are representative of typical star-forming galaxies within the interval $1 < z < 5$. Moreover, circumstantially, the agreement between the EW(Hα) and UV-based sSFR estimates suggests that EW(Hα) could be a reasonable proxy for sSFR at $z \leq 5$, an issue which will be pursued further below.

5.2 The evolution of EW(Hα)

In Fig. 5, we plot the median EW(Hα) for our four galaxy samples against redshift, together with recent determinations of EW(Hα) from the literature. In particular, at $z \leq 2.5$ we plot the spectroscopic results of Fumagalli et al. (2012), Erb et al. (2006) and Kashino et al. (2013), and the narrow-band results of Sobral et al. (2013). In order to ensure a fair comparison, where possible, we have plotted the literature results appropriate for the same stellar mass range as our own data (i.e. $9.5 < \log_{10} M_\star/\,\mathrm{M}_\odot < 10.5$). Where this is not possible, we have scaled the published EW(Hα) values under the assumption that $\mathrm{EW(H}\alpha) \propto M_\star^{-0.25}$ as determined by Sobral et al. (2013).[1] Where necessary, we have converted quoted values of EW(Hα+N[II]) to EW(Hα) by assuming that EW(Hα) = 0.9 ×EW(Hα+N[II]), as recently derived by Sanders et al. (2015) from near-IR spectroscopy.

At higher redshifts ($z \geq 4$), we plot the EW(Hα) results from three previous studies (Shim et al. 2011; Stark et al 2013; Rasappu et al. 2015). As before, we plot the Rasappu et al. (2015) data point with a down arrow, simply because it is based on a sample of galaxies with a significantly lower median stellar mass (see Section 5.3.3). As in Fig. 4, the blue solid line shows the best-fitting EW(Hα)–z relation of the form $\propto (1+z)^{1.0}$, with a normalization set by fitting to our new data points in the range $1 < z < 5$ alone. Likewise, the green dashed line shows an EW(Hα)–z relation with the same functional form as the Speagle et al. (2014) sSFR–z relation, with the appropriate normalization to pass through our new data point at $z \simeq 2.3$. Finally, the black dotted line shows an EW(Hα)–z relation of the form $\propto (1+z)^{1.8}$, as derived by Fumagalli et al. (2012) at $z \leq 1.5$.

5.3 Comparison with previous results

Fig. 5 demonstrates that our new measurements of EW(Hα) at $z \simeq 1.3$ and $z \simeq 2.3$ are in good agreement with previous literature results based on near-IR spectroscopy (e.g. Erb et al. 2006; Fumagalli et al. 2012; Kashino et al. 2013) and narrow-band imaging (e.g. Sobral et al. 2013). It can be seen that at $0 \leq z \leq 2$ a relatively consistent picture emerges, whereby the typical EW(Hα) displayed by $\simeq 10^{10}\,\mathrm{M}_\odot$ star-forming galaxies evolves by a factor of

[1] Note that the EW(Hα) results of Erb et al. (2006), Fumagalli et al. (2012) and Kashino et al. (2013) are all consistent with an $M_\star^{-0.25}$ scaling.

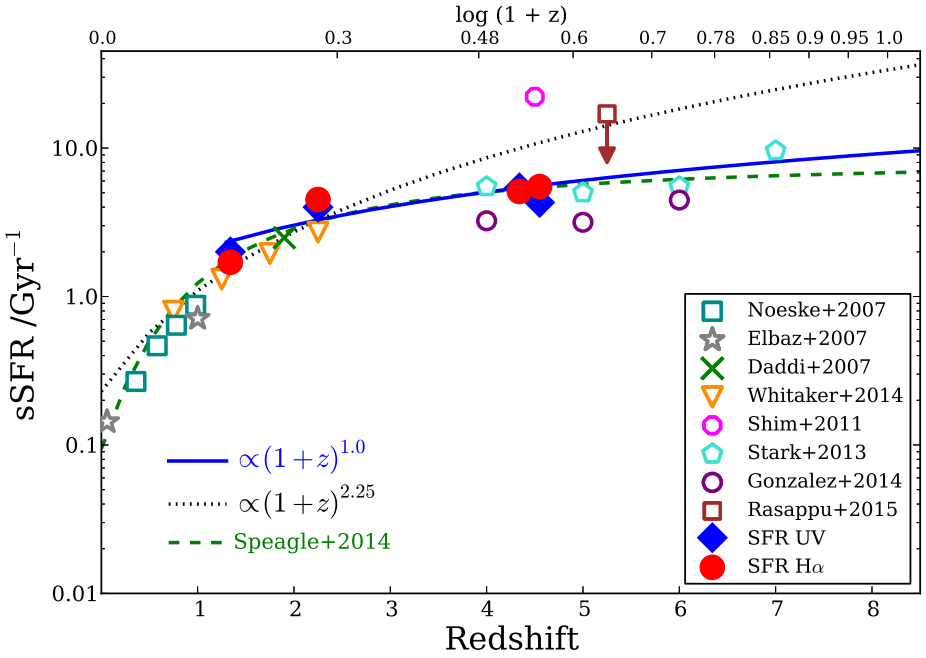

Figure 4. The evolution of sSFR as a function of redshift. The filled blue diamonds and red circles show the median values of sSFR for the four galaxy samples presented in Table 1. The filled blue diamonds show our median sSFR measurements based on UV luminosity, while the filled red circles show the median sSFR measurements as derived from our SED-based measurements of EW(Hα). The results of various different literature studies have also been plotted for comparison. The dotted black line shows sSFR evolution of the form $\propto (1+z)^{2.25}$, as typically predicted by galaxy evolution models (normalized to pass through the cluster of data points at $1 < z < 2$). The dashed green line shows the sSFR–z relation derived by Speagle et al. (2014) for galaxies with stellar mass $\log(M_\star/\mathrm{M}_\odot) = 9.8$, the same as the median mass of our galaxy samples. The blue solid line shows a relation of the form $\propto (1+z)^{1.0}$, which was fitted to our new data points alone (see the text for discussion). It can be seen that our sSFR results, based on two independent measurements, are both internally consistent and in excellent agreement with the sSFR–z relation derived by Speagle et al. (2014) for galaxies of this mass.

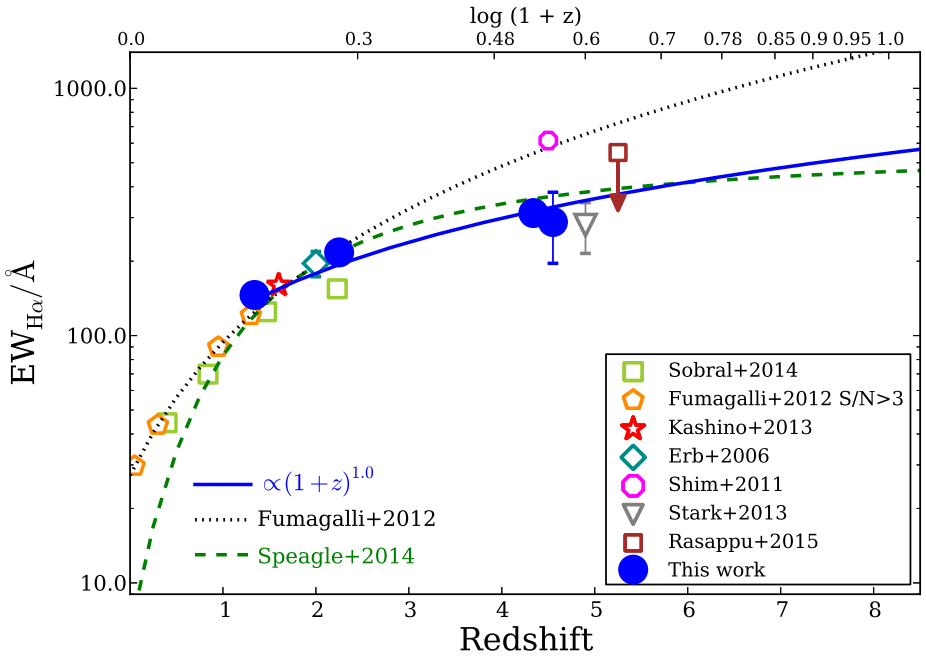

Figure 5. The evolution of EW(Hα) as a function of redshift. The filled blue circles show our SED-fitting-based EW(Hα) measurements (median values) for the four different galaxy samples presented in Table 1. The results of various previous studies from the literature are also plotted for comparison. The grey dotted line shows the evolution extrapolation by Fumagalli et al. (2012), based on galaxies at $z \leq 1.5$ with stellar masses in the range $10^{10-10.5}$ and $S/N > 3$ detections of the Hα emission line in their 3D-HST spectra. The green dashed line shows a fit to our EW(Hα) data assuming the same functional form as the sSFR–z relation derived by Speagle et al. (2014) for a galaxy stellar mass of $\log(M_\star/\mathrm{M}_\odot) = 9.8$ (i.e. green dashed line in Fig. 4). After adopting this fixed functional form, we have simply shifted the normalization of the green dashed line to match our EW(Hα) data point at $z \simeq 2.3$. As in Fig. 4, the blue solid line shows a relation of the form $\propto (1+z)^{1.0}$, which was fitted to our new data points alone (see the text for discussion).

$\simeq$7, reaching a value of $\simeq$200 Å by $z \simeq 2$. In contrast, several recent studies of the evolution of EW(Hα) at $z \geq 2$ have reached apparently contradictory conclusions, with quoted values for the typical EW(Hα) at $z \geq 4$ differing by factors of $\simeq$3. In this sub-section, we compare our new results to those of recent high-redshift EW(Hα) studies and attempt to identify the sources of any discrepancies.

5.3.1 *Shim et al. (2011)*

Shim et al. (2011) performed a very similar SED-based analysis to the work presented here, and derived EW(Hα) values for a final sample of 64 spectroscopically confirmed LBGs in the redshift range $3.8 < z < 5.0$, selected from GOODS-S and GOODS-N fields. In Fig. 5, we have plotted a rest-frame EW(Hα) of 615 Å for Shim et al. (2011), which is the median value for the objects in common with our work, and after applying our estimated correction factor $f = 0.79$ rather than the value of 0.71 quoted in their paper. This number is a full factor of 2 larger than our new EW(Hα) result of $\simeq$300 Å, which clearly requires some explanation. Although Shim et al. (2011) adopted different SED models [i.e. Charlot & Bruzual (2007) models rather than BC03] and considered stellar populations with a lower age limit (i.e. 1 Myr rather than 50 Myr), our tests suggest that straightforward differences in photometry are responsible for the majority of the difference in our final EW(Hα) numbers.

A direct comparison of the photometry for the 19 GOODS-S objects which are common to Shim et al. (2011) and our own $z \simeq 4.5$ spectroscopic galaxy sample indicates that the Shim et al. (2011) IRAC 3.6 μm photometry is systematically $\sim$0.2 mag brighter than the deconfused photometry from Guo et al. (2013). If we artificially brightened our IRAC 3.6 μm photometry by 0.2 mag, this would be sufficient to raise our derived EW(Hα) value to $\simeq$590 Å, in good agreement with the Shim et al. (2011) result. Any remaining difference can likely be attributed to the improved quality of the K_s-band photometry available within the CANDELS UDS and GOODS-S fields from the HUGS survey. Within this context, given that our K_s-band and IRAC photometry should be aperture matched by the TFIT algorithm based on the same H_{160} priors, it seems likely that the EW(Hα) values derived by Shim et al. (2011) could be overestimated by a factor of $\simeq$2.

5.3.2 *Stark et al. (2013)*

Stark et al. (2013) performed an SED-based analysis of 45 spectroscopically confirmed LBGs drawn from GOODS-S and GOODS-N in the redshift interval $3.8 < z < 5.0$ (30 objects in common with Shim et al. 2011). The SED fitting performed by Stark et al. (2013) is even more similar to that performed here, although restricted to 1/5 solar metallicity and allowing ages as low as 5 Myr, and they estimated that the Hα emission line contributed 76 per cent of the observed EW. The final value derived by Stark et al. is EW(Hα) = 270 Å, in good agreement with our new results. Interestingly, the value of 270 Å is derived from their SED fits which *include* the IRAC 3.6 μm photometry, rather than *exclude* it. The figure for EW(Hα) derived by Stark et al. (2013) based on SED fits which exclude the IRAC 3.6 μm photometry is actually 410 Å, $\simeq$40 per cent higher than our new number.

Although it is difficult to be definitive, it seems likely that differences in the available K_s-band photometry are at least partly responsible. From our final sample of 26 spectroscopically confirmed $3.8 < z < 5.0$ galaxies, 15 are in common with the Stark et al. (2013) sample. For this sub-sample, we find that the new HUGS K_s-band photometry is systematically $\simeq$0.15 mag brighter than the ISAAC K_s-band photometry available to Stark et al. (2013). Assuming similar IRAC photometry, this difference alone is likely to explain most of the offset between our new results and those of Stark et al. (2013).

5.3.3 *Rasappu et al. (2015)*

Most recently, Rasappu et al. (2015) presented a study of EW(Hα+[N II]+[S II]) for a sample of star-forming galaxies at $5.1 < z < 5.4$ in the GOODS-N and GOODS-S fields. Based on an SED-fitting analysis (excluding the Hα-contaminated IRAC 4.5 μm filter) of 13 galaxies with spectroscopic redshifts and 11 galaxies with photometric redshifts in this redshift interval, Rasappu et al. find mean EW(Hα+[N II]+[S II]) values of 665 ± 53 and 707 ± 74 Å for the photometric and the spectroscopic samples, respectively. If we simply average these values and assume that Hα contributes $\simeq$ 80 per cent of the total EW(Hα+[N II]+[S II]), this suggests EW(Hα) $\simeq$ 550 Å. Alternatively, the median of the individual EW(Hα+[N II]+[S II]) determinations from Rasappu et al. (2015) is 670 Å, which again leads to EW(Hα) $\simeq$ 550 Å. It is therefore clear that the EW(Hα) results of Rasappu et al. (2015) at $z \simeq$ 5.3 are a factor of $\simeq$ 1.8 higher than our results at $z \simeq 4.5$.

Although apparently inconsistent, it is likely that most of this discrepancy can be attributed to differences in the stellar masses of the galaxies studied here and in Rasappu et al. (2015). After taking into account differences in the assumed IMF, only three galaxies in the Rasappu sample have stellar masses within our adopted range. The median EW(Hα+[N II]+[S II]) for those three galaxies is 310 Å, implying EW(Hα) $\simeq$ 250 Å, in good agreement with our results. In fact, the median mass for the galaxies in their sample is $\log(M_\star/M_\odot) \simeq 9.1$ (Salpeter IMF), $\simeq$0.9 dex lower than the median mass of our $z \simeq 4.5$ galaxy samples (after converting to a Chabrier IMF). If EW(Hα) continues to scale as $\propto M_\star^{-0.25}$, this alone is enough to account for a factor of $\simeq$1.7 difference in the expected EW(Hα). As discussed previously, for this reason we have plotted the Rasappu et al. (2015) data point with a down arrow.

6 THE JOINT EVOLUTION OF sSFR AND Hα EW

In the introduction, we highlighted that one of the reasons for studying the evolution of EW(Hα) was the possibility that it could provide a useful proxy for sSFR at high redshift. Within this context, it is worth remembering that, under the assumption that the relationship between Hα line flux and SFR remains fixed, the sSFR–EW(Hα) relationship might be expected to evolve in concert with the average M/L ratios of main-sequence galaxies. Indeed, the results presented in Table 1 provide some evidence that this is the case over the redshift interval $1 < z < 5$, which sees sSFR (UV based) rise by a factor of $\simeq$2.7 compared to a factor of $\simeq$2.1 increase in EW(Hα) in the same redshift range. However, most of this difference occurs within $1 < z < 2$, with sSFR and EW(Hα) both increasing by very similar amounts with redshift within the range $2 < z < 5$. This is consistent with our finding that the average M/L ratios of main-sequence galaxies with stellar masses of $\simeq 10^{10}\,M_\odot$ change very little between $z \simeq 2.3$ and $z \simeq 4.5$. Moreover, from an empirical perspective, an inspection of the results presented in Figs 4 and 5 suggests that the redshift evolution displayed by sSFR and EW(Hα) is very similar. Motivated by this, in this section we employ two

different methods to investigate the joint evolution of sSFR and EW(Hα).

First, we rely on our new EW(Hα) and sSFR data points at $1 < z < 5$ alone. Our data points in Figs 4 and 5 immediately suggest evolution which should be adequately described by a simply power law of the form $\propto (1 + z)^n$. Indeed, if we fit a power law of this form to our data points alone, we find best-fitting relations of the form

$$\mathrm{sSFR}(z) \propto (1 + z)^{1.2 \pm 0.4} \tag{4}$$

$$\mathrm{EW}(z) \propto (1 + z)^{0.8 \pm 0.2} \tag{5}$$

for the evolution of sSFR and EW(Hα), respectively. As a result, it would seem reasonable to fit the evolution of both quantities using a power law of the form $(1 + z)^{1.0}$, which is shown as the blue solid lines in Figs 4 and 5. Clearly, the simple ratio of these two expressions provides us with a conversion between sSFR and EW(Hα). This leads to a relationship of the form

$$\mathrm{EW}(\mathrm{H}\alpha) = (59 \pm 10) \times \mathrm{sSFR}, \tag{6}$$

where EW(Hα) is measured in Å and sSFR is measured in Gyr^{-1}. It can be seen from Figs 4 and 5 that a relationship of this form provides a reasonably good description of the evolution of both EW(Hα) and sSFR over the redshift interval $1 < z < 5$.

The second approach we adopt is based on the sSFR–z relation from the meta-analysis of Speagle et al. (2014). In Fig. 4, the sSFR–z relation from Speagle et al. (2014) for galaxies with stellar mass $\log_{10}(M_\star/\mathrm{M}_\odot) = 9.8$ is shown as the dashed green line. It can be seen that this functional form provides an excellent match to the observational data over the full $0 < z < 7$ redshift range shown in the figure. Under the assumption that sSFR and EW(Hα) display the same evolution with redshift, we are free to use the same functional form in Fig. 5, choosing to floating the normalization such that the Speagle et al. curve passes through our new data point at $z \simeq 2.3$. Clearly, this functional form actually does a reasonable job of describing the evolution of EW(Hα) over the redshift range $0.5 < z < 5.0$. Again, the ratio of the two dashed green curves shown in Figs 4 and 5 provides us with a conversion between sSFR and EW(Hα). In this case, the resulting relationship is of the form

$$\mathrm{EW}(\mathrm{H}\alpha) = (68 \pm 10) \times \mathrm{sSFR} \tag{7}$$

which can be seen to be in good agreement with the normalization derived from our new data points alone. Based on these results, we would argue that EW(Hα) remains a useful independent tracer of sSFR over the redshift interval $1 < z < 5$, and that the conversion between the two quantities is approximately

$$\mathrm{EW}(\mathrm{H}\alpha) = (63 \pm 7) \times \mathrm{sSFR}. \tag{8}$$

Our finding that EW(Hα) evolves relatively slowly over the redshift interval $1 < z < 5$ is in contrast to at least some previous results in the literature. However, as was discussed in Section 5.3, many of the apparent discrepancies can either be explained by our improved photometry or the effects of trying to compare sSFR/EW(Hα) evolution amongst samples with very different stellar masses. While the median EW(Hα) and sSFR do increase significantly from $z \simeq 1$ to $z \simeq 2$, their evolution from $z \simeq 2$ to $z \simeq 5$ is noticeable less dramatic.

Although measuring EW(Hα) via SED fitting is not trivial, it does possess the distinct advantage of being largely independent of the age, nebular emission and dust uncertainties which plague SED-based measurements of SFR. Fortunately, it will soon be relatively trivial to directly *measure* the EW(Hα) for star-forming galaxies in the redshift interval $0.5 < z < 6.5$ with NIRSpec on the James Webb Space Telescope (JWST). If the evolution follows a steep trend with redshift, such as an extrapolation of the Fumagalli et al. (2012) results (dotted line in Fig. 5), then star-forming galaxies at $z \simeq 6.5$ with stellar masses of $\simeq 10^{10}\,\mathrm{M}_\odot$ should have EW(Hα) $\simeq$ 1000 Å. In contrast, if the evolution of EW(Hα) follows the shallower trend suggested by our new results, the same galaxies should have EW(Hα) $\simeq$ 450 Å.

7 SUMMARY

In this paper, we have presented the results of a study aimed at improving our understanding of how EW(Hα) evolves with redshift and testing whether or not EW(Hα) can be exploited as an independent proxy for sSFR at high redshift.

Based on a sample of star-forming galaxies at $1.2 < z < 1.5$, where it is possible to directly measure EW(Hα) from 3D-HST grism spectroscopy, we first demonstrated that it is possible to reliably measure EW(Hα) via SED fitting of the multiwavelength photometry available in the CANDELS UDS and GOODS-S fields.

Having demonstrated the validity of our technique, we then proceeded to explore the redshift evolution of EW(Hα), using samples of spectroscopically confirmed galaxies at $1.2 < z < 1.5$, $2.1 < z < 2.45$ and $3.8 < z < 5.0$ for which the Hα emission line contaminates the H_{160}, K_s and IRAC 3.6 μm filters, respectively. To improve our high-redshift statistics, we also measured EW(Hα) in a photometric-redshift selected sample of $3.8 < z < 5.0$ star-forming galaxies, finding excellent agreement with the results derived from the spectroscopically confirmed sample. In order to ameliorate potential trends with stellar mass, all of our galaxy samples are restricted to the mass range $9.5 < \log(M_\star/\mathrm{M}_\odot) < 10.5$ and have median masses in the range $9.7 < \log(M_\star/\mathrm{M}_\odot) < 9.8$.

Combining stellar mass estimates derived from SED fitting with measurements of UV luminosity and EW(Hα), we derived two measurements of sSFR for each of our four galaxy samples. Both measurements are found to be consistent, and in excellent agreement with recent determinations of the evolution of the so-called main sequence of star formation. Having demonstrated that our galaxies are fully consistent with being located on the main sequence, we compared our new results for the evolution of EW(Hα) with recent determinations in the literature. We concluded that many of the apparent discrepancies with previous literature results are either caused by simple differences in photometry or by comparing the EW(Hα)/sSFR values of galaxy samples with significantly different stellar masses.

Comparing the evolution of sSFR and EW(Hα), two different methods were employed to demonstrate that sSFR and EW(Hα) are consistent with displaying the same evolution with redshift. Taken together, our new results suggest that EW(Hα)/sSFR evolve relatively slowly ($\propto (1 + z)^{1.0}$), increasing with redshift by a factor of $\lesssim$3 over the redshift interval $1 < z < 5$. We conclude that over the interval $1 < z < 5$, EW(Hα) can serve as a useful independent proxy for sSFR, and that the relative normalization of the two quantities is EW(Hα) = (63 ± 7) × sSFR. If correct, this form of evolution would predict that by $z \simeq 6.5$, galaxies with stellar masses $\simeq 10^{10}\,\mathrm{M}_\odot$ will display an average EW(Hα) of $\simeq$450 Å and have sSFR values of $\simeq$6.5 Gyr^{-1}. Fortunately, it will be possible to obtain accurate measurements of both quantities following the launch of JWST.

ACKNOWLEDGEMENTS

EMQ would like to thank the high-z group at Edinburgh, and Emma Curtis-Lake in particular, for very interesting, supportive and constructive talks. We are grateful to Mattia Fumagalli and David Sobral for providing their published results for a direct comparison. We also thank the referee for suggestions which helped to clarify the text. EMQ and RJM acknowledge the support of the European Research Council via the award of a Consolidator Grant (PI: McLure), while FC acknowledges the support of the Science and Technology Facilities Council (STFC) via the award of an STFC Studentship. JSD acknowledges the support of the European Research Council through the award of an Advanced Grant. The research leading to these results has received funding from the European Union Seventh Framework Programme (FP7/2007-2013) under grant agreement no. 312725 (ASTRODEEP). This work uses data from the following ESO programmes: 181.A0717, 186.A-0898. This work is based on observations taken by the CANDELS Multi-Cycle Treasury Program and the 3D-HST Treasury Program (GO 12177 and 12328) with the NASA/ESA HST, which is operated by the Association of Universities for Research in Astronomy, Inc., under NASA contract NAS5-26555.

REFERENCES

Brammer G. B. et al., 2012, ApJS, 200, 13
Bruzual G., Charlot S., 2003, MNRAS, 344, 1000 (BC03)
Calzetti D., Kinney A. L., Storchi-Bergmann T., 1994, ApJ, 429, 582
Calzetti D., Armus L., Bohlin R. C., Kinney A. L., Koornneef J., Storchi-Bergmann T., 2000, ApJ, 533, 682
Cimatti A. et al., 2002, A&A, 392, 395
Cooper M. C. et al., 2012, MNRAS, 425, 2116
Cullen F., Cirasuolo M., McLure R. J., Dunlop J. S., Bowler R. A. A., 2014, MNRAS, 440, 2300
Curtis-Lake E. et al., 2013, MNRAS, 429, 302
Daddi E. et al., 2007, ApJ, 670, 156
Davé R., Oppenheimer B. D., Finlator K., 2011, MNRAS, 415, 11
de Barros S., Schaerer D., Stark D. P., 2014, A&A, 563, A81
Dutton A. A., van den Bosch F. C., Dekel A., 2010, MNRAS, 405, 1690
Elbaz D. et al., 2007, A&A, 468, 33
Erb D. K., Steidel C. C., Shapley A. E., Pettini M., Reddy N. A., Adelberger K. L., 2006, ApJ, 647, 128
Fontana A. et al., 2014, A&A, 570, A11
Fumagalli M. et al., 2012, ApJ, 757, L22
Galametz A., Grazian A., Fontana A., Ferguson H. C., the CANDELS Team, 2013, ApJS, 206, 10
González V., Labbé I., Bouwens R. J., Illingworth G., Franx M., Kriek M., Brammer G. B., 2010, ApJ, 713, 115
González V., Bouwens R., Illingworth G., Labbé I., Oesch P., Franx M., Magee D., 2014, ApJ, 781, 34
Grogin N. A., Kocevski D. D., Faber S. M., the CANDELS Team, 2011, ApJS, 197, 35
Guo Y., Ferguson H. C., Giavalisco M., Barro G., the CANDELS Team, 2013, ApJS, 207, 24
Johnston R., Vaccari M., Jarvis M., Smith M., Giovannoli E., Häußler B., Prescott M., 2015, MNRAS, 453, 2540
Karim A. et al., 2011, ApJ, 730, 61
Kashino D. et al., 2013, ApJ, 777, L8
Kennicutt R. C., Evans N. J., 2012, ARA&A, 50, 531
Koekemoer A. M. et al., 2011, ApJS, 197, 36
Koprowski M. et al., 2016, MNRAS, 458, 4321
Kümmel M., Walsh J. R., Pirzkal N., Kuntschner H., Pasquali A., 2009, PASP, 121, 59
Laidler V. G. et al., 2007, PASP, 119, 1325
Le Fèvre O. et al., 2004, A&A, 428, 1043
McLeod D. J., McLure R. J., Dunlop J. S., Robertson B. E., Ellis R. S., Targett T. A., 2015, MNRAS, 450, 3032
McLure R. J. et al., 2011, MNRAS, 418, 2074
McLure R. J. et al., 2013, MNRAS, 428, 1088
Madau P., 1995, ApJ, 441, 18
Madau P., Dickinson M., 2014, ARA&A, 52, 415
Madau P., Pozzetti L., Dickinson M., 1998, ApJ, 498, 106
Meurer G. R., Heckman T. M., Calzetti D., 1999, ApJ, 521, 64
Mignoli M. et al., 2005, A&A, 437, 883
Mobasher B. et al., 2015, ApJ, 808, 101
Morris A. M. et al., 2015, AJ, 149, 178
Neistein E., Dekel A., 2008, MNRAS, 383, 615
Noeske K. G. et al., 2007, ApJ, 660, L43
Oke J. B., 1974, ApJS, 27, 21
Oke J. B., Gunn J. E., 1983, ApJ, 266, 713
Popesso P. et al., 2009, A&A, 494, 443
Rasappu N., Smit R., Labbe I., Bouwens R., Stark D., Ellis R., Oesch P., 2015, preprint (arXiv:e-prints)
Reddy N. A. et al., 2015, ApJ, 806, 259
Renzini A., Peng Y.-j., 2015, ApJ, 801, L29
Sanders R. L. et al., 2015, ApJ, 799, 138
Schaerer D., de Barros S., 2009, A&A, 502, 423
Shim H., Chary R.-R., Dickinson M., Lin L., Spinrad H., Stern D., Yan C.-H., 2011, ApJ, 738, 69
Sobral D., Smail I., Best P. N., Geach J. E., Matsuda Y., Stott J. P., Cirasuolo M., Kurk J., 2013, MNRAS, 428, 1128
Speagle J. S., Steinhardt C. L., Capak P. L., Silverman J. D., 2014, ApJS, 214, 15
Stark D. P., Ellis R. S., Bunker A., Bundy K., Targett T., Benson A., Lacy M., 2009, ApJ, 697, 1493
Stark D. P., Schenker M. A., Ellis R., Robertson B., McLure R., Dunlop J., 2013, ApJ, 763, 129
Tasca L. A. M. et al., 2015, A&A, 581, A54
Vanzella E. et al., 2008, A&A, 478, 83
Whitaker K. E., van Dokkum P. G., Brammer G., Franx M., 2012, ApJ, 754, L29
Whitaker K. E. et al., 2014, ApJ, 795, 104

This paper has been typeset from a TEX/LATEX file prepared by the author.